Simulation of dynamic orofacial movements using a constitutive law varying with muscle activation

Journal:	*Computer Methods in Biomechanics and Biomedical Engineering*
Manuscript ID:	GCMB-2009-0152.R1
Manuscript Type:	Special Issue Paper
Date Submitted by the Author:	
Complete List of Authors:	Nazari, Mohammad; Grenoble INP, GIPSA Lab Perrier, Pascal; Grenoble INP, CNRS UMR 5216, GIPSA-lab, Speech and Cognition Department Chabans, Matthieu; Grenoble INP, GIPSA-lab, Speech and Cognition Department Payan, Yohan; Université Joseph Fourier - CNRS UMR 5525, Equipe GMCAO - Laboratoire TIMC-IMAG
Keywords:	face biomechanics, orofacial movements, muscle active force, hyperelastic modelling

Simulation of dynamic orofacial movements using a constitutive law varying with muscle activation

NAZARI Mohammad Ali[1,2], PERRIER Pascal[1], CHABANAS Matthieu[1] and PAYAN Yohan[3]

1. GIPSA-lab, Speech and Cognition Department, CNRS UMR 5216 / Grenoble Institute of Technology, France
2. Mechanical Engineering Department, Faculty of Engineering, University of Tehran, Iran
3. TIMC-IMAG, CNRS UMR 5525 / Université Joseph Fourier, Grenoble, France[1]

Correspondance: Mohammad Ali NAZARI, GIPSA-lab Département Parole & Cognition, Domaine universitaire BP 46, 38402 Saint Martin d'Hères, France

This paper presents a biomechanical model of the face to simulate orofacial movements in speech and non-verbal communication. A 3D finite element model, based on medical images of a subject, is presented. A hyperelastic Mooney-Rivlin constitutive law accounts for the non linear behaviour of facial tissue. Muscles fibres are represented by piece-wise uniaxial tensile elements, which generate force. The stress stiffening effect, an increase of the stiffness of the muscles when activated, is modelled by varying the constitutive law of the tissue with the level of activation of the muscle. A large number of facial movements occurring during speech and facial mimics are simulated. Results show that our modelling approach provides a realistic account of facial mimics. The differences between dynamic versus quasi-static simulations are also discussed, proving that dynamic trajectories better fit experimental data.

Keywords: face biomechanics; orofacial movements; muscle active force; hyperelastic modelling.

1. Introduction

Orofacial gestures, produced by articulators such as the tongue, jaw and lips, are of primary importance in speech communication. By their position at the extremity of the vocal tract, lips have a major influence on the acoustic signal generated by the airflow coming from the lung. In addition, seeing facial gestures directly influence the perception of speech. Listeners perceive and interpret the produced speech via a combination of auditory and visual processing, a strategy well demonstrated by the well-know McGurk effect (McGurk and MacDonald 1976).

[1] Currently in PIMS, CNRS UMI 3069 / University of British Columbia, Vancouver, Canada

Consequently an important field in speech communication research is the development of synthetic models of the human face. The accuracy of these models is a major requirement, both for production and perception of speech. In this context, due to the strong influence of 3D lip horn geometry on the spectral characteristics of speech signals, special attention has to be devoted the modelling of the lips region. Moreover, it has been shown that the dynamic of the movements is very important in the perception of facial expressions (Munhall and Vatikiotis-Bateson 1998; Ambadar et al. 2005). Hence, synthetic speaking faces have to well account for the temporal course of face shaping.

Contrary to empirical models based on recorded data or medical images (for example Lucero et al. (2005) or Badin et al. (2008)), our approach in the last decade has been to develop biomechanical models of speech articulators, which are as close as possible to the human anatomy and functional morphology. Special emphasis has been given to the representation of the muscular structures and the rheological properties of soft tissues. Another major contribution has dealt with the motor control system involved in the production of speech and orofacial movements: which muscles have to be contracted to obtain a given acoustic signal or facial mimic? What must be the intensities, variations and sequencing of the motor commands? Former works were focused on a biomechanical modelling of the tongue, first in 2D then in 3D, and the controlled activation of its muscles to generate complex articulatory paths (Payan and Perrier 1997; Perrier et al. 2003; Buchaillard et al. 2009). In continuation of these works, this paper presents a biomechanical model of the face which enables the generation of facial movements in response to muscles activations. The bases of the finite element model (mesh, mechanical properties and boundary conditions), which represent the passive tissues of the face, are presented in section 2. Then, section 3 is

entirely focused on the active components, namely the muscles: their representation, mechanism of contraction, and the evolution of their mechanical properties with activation. Simulations of different orofacial movements are presented in section 4, before the discussion and conclusion.

2. Main structure of the model

Many physically-based models of the human face were developed in the framework of computer graphics facial animation (Lee et al. 1995; Sifakis et al. 2005), computer aided surgery (Chabanas et al. 2003; Gladilin et al. 2004) or speech production study (Lucero and Munhall 1999; Gomi et al. 2006).

The pioneer work of Lee et al. (1995) has made popular a discrete modelling framework, with sparse mass-spring entities regularly assembled inside facial tissues. This approach allows fast computations with a simple algorithmic implementation. However, in addition to the lack of accuracy of such models and to their numerical instabilities, it seems to be very difficult to set their elastic parameters (the stiffness of springs) in order to fit the constitutive behaviour that is observed and measured on living tissues. Recently Kim & Gomi (2007) have improved Gomi et al.'s (2006) discrete model by implementing a so-called "continuum compatible" mass-spring model with stiffness parameters that can be adjusted in order to follow a simple linear continuum constitutive law. Although this model is interesting in computational terms, especially for dynamic simulations, it is limited to correctly reproduce the behaviour of highly non-linear material such as facial tissues (Fung 1993; Gerard et al. 2005).

In continuity with the works of Chabanas et al. (2003) and Sifakis et al. (2005), we have chosen to use the Finite Element method to model the continuous tissues of the human face (Groleau et al. 2007; Nazari et al. 2008). Although

computationally less efficient, it enables in particular the use of non linear mechanical modelling such as hyperelastic laws to better approximate the tissues behaviour (Humphrey and Yin 1989; Weiss et al. 1996; Yucesoy et al. 2002; Blemker et al. 2005).

Our implementation is based on the ANSYS ® release 11.0 software.

2.1 Mesh of the passive tissues

The main mesh is a Finite Element (FE) discretization of the volume defined by the facial tissues located between the skull and the external skin surface of the face. It is based on a previous continuous face model developed by Chabanas et al. (2003) in the context of computer aided maxillo-facial surgery. The outer and inner surfaces of the mesh were extracted from a CT scan of a female adult subject. The volume delimitated by these two surfaces was then manually meshed, as regularly as possible, with hexahedral and wedge elements (figure 1). Anatomically, the face can be considered as the superposition of three distinct layers of tissues, namely (from the internal to the external layer) the hypodermis, dermis and epidermis (Stranding 2005). The mesh is thus also built in three discrete layers of elements. The external one corresponds to the epidermis (very thin) and dermis parts while the two internal layers model the hypodermis, which will later include the facial musculature (section 3). The mesh is composed of 6342 brick elements (6024 hexahedron and 318 wedges) based on 8720 nodes. In order to reduce the number of DOF during simulation the mesh was assumed to be symmetrical along the sagittal plane, which seems reasonable in the context of speech production.

------ Figure 1 around here ------

2.2 Mechanical properties

Element material properties are assumed to follow a hyperelastic law (Fung 1993). A simplified 5 parameters Mooney-Rivlin model is used, which is based on a strain-energy function W defined by:

$$W=c_{10}(I_1-3)+c_{01}(I_2-3)+c_{20}(I_1-3)^2+c_{11}(I_1-3)(I_2-3)+c_{02}(I_2-3)^2+((J-1)^2/d) \quad (1)$$

where I_1 and I_2 are respectively the first and second invariants of the right Cauchy-Green strain tensor, J is the determinant of the elastic deformation gradient, and $d=(1-2v)/(c_{10}+c_{01})$ with v the Poisson's ratio. The derivatives of W with respect to strain give stress:

$$S_{ij}=2\partial W/\partial C_{ij} \quad (2)$$

S_{ij} are the components of the second Piola-Kirchhoff stress tensor and C_{ij} the components of the right Cauchy-Green deformation tensor.

In our work, a simplified version of the strain-energy function W is used with only two constants, c_{10} and c_{20}, different from zero (Gerard et al. 2005; Buchaillard et al. 2009). According to Tracqui and Ohayon (2004), $c_{10}\approx E/6$ where E is the Young's modulus. The two coefficients c_{10} and d have been calculated from the values reported in Payan and Perrier (1997), with the assumption of mechanical linearity and incompressibility of tissues, namely $E=15$ kPa and v=0.499. The c_{20} coefficient has been adapted from the values proposed for tongue tissues by Buchaillard et al. (2009) based on indentation measures from a cadaver's tongue (Gerard et al., 2005). The computed constants are shown in table 1.

------ Table 1 around here ------

The modelled passive tissues have been so far considered as homogeneous and isotropic. It could be improved in future works, especially by setting specific

mechanical properties to the different layers of the mesh. The mechanical properties of the active part of the model, the muscles, will be treated in section 3.4.

2.3 Boundary conditions and contact surfaces

Nodes of the internal layer of the mesh corresponding to the face tissue attachments to the skull are fixed. Others are free.

During speech and facial mimics, many contacts occur between the upper and lower lip, and between the lips and the teeth. They are extremely important in lips shaping. The teeth surfaces on mandible and maxilla, segmented on CT images, have been approximated with spline surfaces, and then meshed with quadrilateral undeformable elements (figure 2). Contacts are handled using surface to surface contact elements (CONTA173 and TARGE170 in Ansys ®), which provide collision detection and sliding reaction, considered here without friction (MU=0). There is no initial interpenetration between all the contact surfaces.

------ Figure 2 around here ------

3. Muscles

Since orofacial movements are directly generated by facial muscles, a realistic modelling of their course and mechanical properties is a main challenge. The total force generated in a muscle is the sum of two components: an active (F_{ac}) one and a passive (F_{pc}) one. Due to α-motoneurons depolarization, muscle fibres generate force, which in turn causes change in muscle length. The force generated through the actin-myosin cross-bridges is the active component of muscle force. Due to their stiffness the surrounding tissues will resist to the active component thus defining a passive component of muscle force. In real muscles this passive component is not isotropic

since the mechanical properties in the direction of muscle collagen fibres are different from the embedding matrix (McMahon 1984). Hence, the passive material behaviour should be modelled with a transversely isotropic material (Humphrey and Yin 1989; Weiss et al. 1996; Yucesoy et al. 2002; Blemker et al. 2005). However, in a first approach, this behaviour is considered as isotropic.

The very earlier model of the active part of muscle force was proposed by Hill (1938). According to this basic model a contractile element generates force as a function of muscle length (F versus L curve) and its velocity (F versus V curve). These curves are assumed to be scaled up or down as a function of the level of activation (Zajac 1989). More recently, authors working with finite element framework have modelled the muscle force by designing new elements which include both active stress stiffening effect and passive transversal isotropy (Wilhelms-Tricario 1995; Blemker et al. 2005). These elements need to be oriented along the axis of isotropy (Ng-Thow-Hing and Fiume 2002) to define fibre and cross fibre directions and also they should be distinguished from the surrounding tissues (Teran et al. 2005). This method has been implemented by Sifakis et al. (2006) for modelling face muscles and speech behaviours quasi-statically.

Next subsections present the muscle modelling developed in our work, with the representation of their active and passive components and the stress stiffening effect, leading to an evolution of the mechanical properties of muscles during contraction.

3.1 Muscle contractile fibres or active part

The muscular structure of the face enables huge possibilities of movements, in speech, eating and facial expressions, with a great dexterity. Its complex structure can be divided in two groups of muscles (Stranding 2005). Muscles of mastication are the

deep, strong muscles that generate the movement of the mandible. Since the mandible is not handled yet in our modelling, we have only focused on the other group, the muscles of the lip region, namely the superficial muscles involved in facial mimics (Hardcastle 1976). Most of them are bilateral, symmetrical, gathered around the lips with one bony insertion and the other within the facial tissues. A notable exception is the orbicularis oris, a specific constrictor muscle embedded in the lips without bony insertions.

In order to ensure anatomical and physical reliability, muscles courses and insertions were directly defined from medical images and anatomical charts, with the help of a maxillofacial surgeon. The locations of points describing the muscle fibres were measured in the different CT scan slices. The number of fibres per muscle depends on its extent and size. Figure 3 and table 2 show the ten orofacial muscles that are modelled.

------ Figure 3 around here ------

------ Table 2 around here ------

Muscle fibres are embedded in the facial mesh as continuous sets of uniaxial cable elements. Since each cable is a line in 3D space, their number per fibre increases as a function of the muscle fibre curvature, to model this curvature smoothly. These cable elements (LINK10 in Ansys®) act in tension only and will become slack under compression. Such properties are consistent with the observations that in the fibre direction a muscle can resist only tensile forces and not compressive forces (Loocke et al. 2006).

End points of the cable elements are defined independently of the level of refinement of the main mesh. They correspond to anatomical landmarks located in reference to the skull. This approach enables to refine or modify the mesh without

requiring any change in the definition of muscles courses. To couple the fibres with the main mesh, *point to surface* contact elements are used. The *points* (pilot nodes) are the extremities of the cable elements. They are bilaterally linked to the *surfaces* of the mesh elements which centroids are the closest to the cable extremity. Figure 4 displays the cable elements and the corresponding coupling elements for the muscles in half of the face. The no-displacement boundary condition is also applied to the ends of cable elements that correspond to the muscles insertions on the skull.

------ Figure 4 around here ------

3.2 Muscle body or passive part

Once the fibres are set, the body of the muscles can be defined in the main mesh. A neighbourhood is determined around each fibre by an algorithm considering a sphere, which radius is equal to an estimation of the muscle cross-sectional dimension, running along the cable elements lines. Each element of the main mesh intersecting the sphere is then labelled as a part of the muscle body. The resulting bodies of the muscles in the mesh are displayed in figure 5 for the left half of the face. Although this definition of the muscle body is a rough approximation, it is enough so far for our use, which is to account for the stress stiffening effect.

------ Figure 5 around here ------

3.3 Stress stiffening effect

Muscles behave like a transversely isotropic material, with an isotropic behaviour in the directions orthogonal to the muscle fibres. This means that mechanical properties in the direction of muscle fibres are different from the ones in the cross-fibre direction. Due to force generation in the fibres direction and to the

fibres tensile characteristics, the transversal bending stiffness increases with the tensile force (similarly to the stress stiffening phenomenon in cable members or membranes).

------ Figure 6 around here ------

This is illustrated in Figure 6 with a simple example of a virtual point P inside a muscle fibre originally at equilibrium under constant muscle activation (force F_1) and then displaced (by δ) because of the action of a force F applied in the muscle transversal direction. Once the new equilibrium is reached (Figure 6 lower panel), assuming a linear relationship between force and displacement, we have:

$$F = 2F_1 \frac{\delta}{\ell_1} \left(\frac{1}{\sqrt{1+\left(\frac{\delta}{\ell_1}\right)^2}} \right) \qquad (3)$$

This means that, when δ is negligible as compared to ℓ_1, the muscle transversal stiffness $dF/d\delta$ is proportional to muscle force F_1.

When a muscle is activated, its fibres generate forces that resist to elongation, according to a certain tension-length relation (see for example McMahon (1984)), and in a way that increases when activation increases (see for example Wilhelms-Tricario (1995)). In real muscle the fibres distribution is so dense, that the resistance to elongation of the whole muscle body increases with elongation in the fibres direction. In our model, muscle fibres are not represented in all their details. They are modelled by a limited number of *localized* macrofibres (typically from one to three). When the muscle is activated, each of these macrofibres generates a force and resists to the elongation, but since the fibres are localized, this resistance does not apply to the whole body of the muscle. This would not be a realistic behaviour. In order to compensate for this drawback, the stiffness in the body elements of the muscles

(section 3.2) increases with muscle activation in the fibres directions. Hence, muscle activation is associated both with a resistance to stress in the direction orthogonal to the fibre direction (the stress stiffening effect) and with a resistance to elongation in the fibre direction. Consequently, it is modelled by an isotropic increase of the tissues stiffness, implemented by modifying the parameters of the passive constitutive law (equation 1), according to the approach explained in the next section.

3.4 Implementation of muscle activation and stress stiffening effect

The cable elements generate the active force F_{ac} of each muscle, following the relation:

$$F_{ac}=AE_{cable}\,(\varepsilon-\alpha\Delta T) \qquad (4)$$

where A is the cable cross sectional area, ε its strain and E_{cable} its Young's modulus. In standard ANSYS ® use, parameter T is equivalent to the temperature of the element, and α to the thermal coefficient of expansion of the cable. In our case, we have used parameters T and E_{cable} to specify the *level of activation*. Parameter E_{cable} is a scaling factor specifying the maximal level of activation, which is muscle specific. Parameter T is used to control the *level of activation* within the muscle specific maximal range of variation. Thus, parameter T can be considered as a *normalized control parameter of muscle activation*. Decreasing T leads to a shortening of the cables lengths, which therefore exert forces on the main mesh through the coupling elements. The activation level is then a decreasing function of parameter T. The value of α is arbitrarily set to 0.001

To account for the stress stiffening effect, the constitutive law of the elements of a muscle body varies with the level of muscle activation specified with T. In agreement with Buchaillard et al. (2009), parameters c_{10} and c_{20} of the passive

hyperelastic law are hence linearly scaled as an increasing function of the activation, which is a decreasing function of T (Figure 7).

------ Figure 7 around here ------

When different muscles are activated simultaneously, the stiffness of the main mesh elements which are common to these muscles' bodies change as a function of the most activated muscle, and not as the result of an accumulation of the stiffness changes associated with each individual muscle activation. The proposed stress stiffening modelling is functionally correct, except for the resistance to compression in the fibres direction. Indeed, it is known that this resistance varies with the strain rate and is close to zero when this rate is low (Loocke et al. 2006). Further improvements will be provided along this line in future works.

The muscle activationvaries in time as a ramp function. In further works that we will develop in the context of speech production, these commands will be handled by a motor control mechanism integrating voluntary commands and low-level feedback information sent by the muscles (Feldman 1986; Buchaillard et al. 2006).

3.5 Dynamic parameters

For dynamic transient analysis, viscosity is modelled using proportional damping:

$$\boldsymbol{C}=\alpha\boldsymbol{M}+\beta\boldsymbol{K} \qquad (5)$$

To determine α and β coefficients the first 7000 modes of the main mesh (about a third of the total number of degrees of freedom) were calculated. Simulations were run twice, first with the material stiffness used in the absence of muscle activation and then for a high material stiffness level (10 times more). The corresponding natural frequencies vary from 0.5 Hz up to 15 Hz. Within this interval, parameters α and β

have been tuned such that the damping ratio (ratio of viscous damping factor to critical damping) is larger than and near to one. The computed values are $\alpha=19\ sec^{-1}$ and $\beta=0.055\ sec$.

The density of face tissues is set to $\rho=1.04E^{-6}$ kg/mm^3 (Buchaillard et al. 2006). The effect of gravity has not been considered.

Other parameters regarding solver and computational costs are discussed in the appendix.

4. Simulations and results

Different muscle activation patterns have been used and their influences on facial gestures and mimics evaluated. Both static and transient analyses have been performed. In addition to the static analysis that takes into account only the stiffness matrix, dynamic simulations obtained with full transient analysis also takes into account the effect of inertia and viscosity.

4.1 Simulation of facial mimics resulting from various orofacial gestures

Activation of muscles taken individually and in coordination has been investigated. In this section, only the final shapes of the mesh resulting from these activations are shown. They are the same for the static and the full transient analysis. These results well comply with the anatomical predictions in the related literature (Standring 2005).

The result of activating zygomaticus draws the angle of the mouth upwards and laterally (Figure 8).

------ Figure 8 around here ------

Levator labii superioris elevates the upper lip. Acting with other muscles, it modifies the nasolabial furrow. In some faces, this furrow is a highly characteristic feature often deepened in expressions of sadness or seriousness. The activation of the levator labii superioris with zygomaticus and levetor labii superioris alaeque nasi in Figure 9 well satisfies that hypothesis.

------ Figure 9 around here ------

The effect of orbicularis oris peripheralis (OOP) in protruding and rounding the lips has been shown (Figure 10). The effect of stiffening in producing rounding with protrusion has been discussed in Nazari et al. (2008): without the stiffening, lips are protruded but the amount of lip opening is too large.

------ Figure 10 around here ------

Figure 11 shows the consequence of the activation of the risorius and Figure 12 the impact of activation of the buccinator (BUC). In Figure 13 the mimic associated with the coordinated action of OOP and BUC is illustrated. In all these figures these actions are qualitatively consistent with predictions made from anatomical knowledge.

------ Figure 11 around here ------

The risorius is known to stretch the mouth laterally and to retract the corners of the mouth. This is consistent with the strain depicted in Figure 11.The buccinator has no or little influence on the lips, and essentially compresses the cheeks against the teeth (Blanton et al. 1970). Our simulation matches quite well these expectations (Figure

12): the lips have the same shape as in our model at rest, while the strain essentially affects the lower part of the face.

------ Figure 12 around here ------

The OOP has been shown in our model to generate a protrusion and a closing of the lips which is consistent with usual hypotheses in the literature (Gomi et. al 2006; Nazari et. al 2008). Meanwhile, the coordinated action of the buccinator and the OOP generates a closing of the lips only. It can be assumed that the stiffening of the cheeks due to the buccinator activation limits the amplitude of the lip protrusion, which would explain that mainly closure is observed.

------ Figure 13 around here ------

4.2 Dynamics versus Quasi-static simulations

We have studied the effect of dynamic versus quasi-static analysis on the lip protrusion. For this purpose both OOP and mentalis (MENT) muscles are activated. The same activation level in both dynamic and static analyses is assumed. Figure 14 shows the trajectories, for both conditions, of a node located on the lower lip in the midsagittal plane.

------ Figure 14 around here ------

While starting and ending points are the same in static and dynamic analysis, the trajectories are clearly different. The trajectory obtained with the static analysis is close to a straight line while the dynamic trajectory is noticeably curved. This difference is large enough to generate significant differences in lip shape variation from the starting point to the ending point, and then to significantly influence the

acoustic signal. In addition, a large number of human skilled movements have been shown to follow curved path (Morasso, 1981).

Figure 15 shows the tangential velocity profile for the same point together with the corresponding activation signal..

------ Figure 15 around here ------

An asymmetrical bell-shaped velocity pattern is generated. This kinematic pattern is typical for lip movements as shown for example by Shaiman et al. (1997) for several American English speakers.

Both properties, the curved path and the bell-shaped velocity profiles, observed in experimental studies and accounted for in dynamic analysis and not in quasi-static analysis demonstrates the necessity to integrate dynamic factors, such as inertia and damping, to obtain realistic simulations of lip shape variations in speech production.

To assess more precisely the realism of the trajectories produced by our model, they can be compared to lips trajectories measured with video processing (Abry et al. 1996) from a native speaker of French. As an illustration, let us consider the sequence /iRy/ embedded in the carrier sentence‘Tu dis “ruise” (/tydiRyiz/, you’re saying “ruise”, /). These data were processed with a low-pass linear phase filter (cut-off frequency 6 Hz). The trajectory of a point located on the lower lip in the mid-sagittal plane has been extracted in the temporal section corresponding to lip protrusion from /i/ to /y/ (Figure 16). It can be observed that the path of this point is qualitatively similar to the path simulated with dynamic analysis (Figure 14). More specifically, the path is curved, a key feature that could not be predicted from the pseudo-static analysis.

------ Figure 16 around here ------

Figure 17 shows the experimental velocity profile: it has, like our simulation, an asymmetrical bell-shape in agreement with Shaiman et al.'s (1997) data collected from speakers of American English.

------ Figure 17 around here ------

This example of a comparison between simulations and real data confirms the general observation made above: contrary to those obtained in the quasi-static analysis framework, the simulations obtained in the dynamic analysis framework generate curved paths and bell-shaped velocity profiles similar to those observed in experimental lips protrusion movements collected during speech production

The experimental movement and the simulation in dynmica analysis have also similar ranges of velocity (maximum velocity 3.9cm/s *versus* 2.4cm/s), durations (200ms *versus* 270ms at 20% of the peak velocity), and movement amplitudes (4.5mm versus 4mm for the horizontal protrusion).

Some discrepancies can be noticed between simulations and experimental data. In the experimental data, the curved path includes a rising part followed by a short decline. In the simulation this rising/declining sequence is also observed, but it is preceded by a horizontal part. It is important to state that these differences are not intrinsically due to the characteristics of the model but ,more factually, to differences between the conditions of simulation and the conditions of real speech production. In the simulations the movement starts from a zero velocity position and ends at a zero velocity position, while experimental data were extracted from a longer speech

continuum (Figure 16) in which the observed section does not start or end with a zero velocity position. This phenomenon can be clearly seen in the experimental velocity profile (Figure 17), in which velocity curve never crosses zero.

5. Discussion and conclusion

The use of a realistic dynamical biomechanical model of the face has allowed simulating a number of facial movements comparable to those occurring during the production of speech or of facial mimics in non-verbal communication.

One of the main specificities in our model is the representation of the muscles. First, their anatomical description, which relies on subject specific medical images and anatomical data, is independent from the finite element mesh. It enables to easily modify the structure of the mesh, its number or type of elements, without losing the anatomical information. The second aspect that makes our model original is the modelling of elastic muscle properties and more specifically the stress stiffening effect associated with muscle activation. The elastic characteristics are inherent to the muscle body definition, and are determined by varying the constitutive law of the muscle's tissues with the level of activation of the muscle. Results on the protrusion movement have shown that this approach enhances the generation of accurate facial movements and shapes (Nazari et al., 2008).

Studies in the literature have shown that articulatory dynamics has a major impact on the temporal patterning of speech movements. Time characteristics are important in speech perception. We have shown that lip movement patterns are indeed different in quasi-static and dynamic simulation frameworks. Interesting results, close to experimental observations, have been obtained for the dynamic framework, and not

for the quasi-static one, such as the generation of curved paths and bell-shaped velocity profiles classically observed in unperturbed skilled human movements (Morasso 1981). The clear differences observed between the trajectories simulated with dynamic and static analysis demonstrate that the usage of dynamic analysis is a requirement for speech production studies. The role of dynamics has also been studied in the literature for non-speech movements. Ambadar et al. (2005) observed for example that recognition of subtle facial expressions by watching the evolution of facial gestures in time is much easier than by looking at static shots. Hence, in modelling studies, if temporal patterning of movements integrates dynamic constraints like inertia and viscosity, synthetic facial expressions will be deciphered faster and easier.

Simulations have also highlighted the indirect role of stiffening the face, mostly in the cheeks area, on the way muscles impact the lip shapes. It was shown that the stiffening of the cheeks due to the activation of the buccinator induces a limitation of the amplitude of the upper lip protrusion associated with OOP activation. The role of muscles, which are not directly involved in lip shaping, was thus demonstrated. These results, similar to those of Buchaillard et al. (2009) about the role of mouth floor muscles in tongue elevation, are encouraging for our modelling approach toward a better understanding of facial mimic mechanisms.

Future improvements of the model will among others concern the mechanical properties, to account for the non-homogeneity of the tissue layers, and include some mesh refinement. Also, new muscle elements will be developed to integrate the displacements and strain dynamically in their constitutive law. This will be used while implementing a motor control mechanism that integrates voluntary commands and low-level feedback. This mechanism will handle the activation commands sent to

every muscle to reach specific targets, defined as positions or shapes of the face in relation with specific spectral patterns of the acoustic signal. Other works will concern the coupling of the face with a model of the jaw. Finally, experimental data will be more extensively used to better evaluate, qualitatively and/or quantitatively, the simulated orofacial movements.

Appendix

The sparse direct solver based on Newton-Raphson method has been used. Convergence is assumed when

$||\Delta V|| < \varepsilon_V V_{ref}$

where V is the variable, which is in our case either force or displacement, ε_V is the tolerance and $||\Delta V||$ the Euclidian norm of the variable difference at each time step (ANSYS Inc., Theory Reference). The assumed values are given in Table 3.

----Table 3 around here--------

In the Newton-Raphson method, line search with adaptive descent is used. The computation time on a Windows XP (32bit) platform running on a machine with a Duo CPU E6850 @ 3 GHz for static analysis is around 3000 seconds per simulation (3183 CPU times) and for dynamic analysis is around 20,000 seconds (10,000 CPU times) for simulation of one second real time gesture.

Acknowledgement

We are pleased to express our gratitude to Dr. Pierre Badin, Dr. Christophe Savariaux and Dr. Jean Luc-Schwarz for providing us with experimental movement data from different subjects.

FIGURES CAPTIONS

Figure 1: Main mesh of the face soft tissue.

Figure 2: Surfaces of contact elements between lips (a) and lips and teeth (b).

Figure 3: Macrofibers defining the muscles of the face shown in CT data (a), in the main mesh (b), and with their abbreviated names (c).

Figure 4: Coupling elements between the piece-wise fibres of cable elements and the main mesh (only the left half of face is shown).

Figure 5: Body of the muscles: elements of the main mesh in a neighbourhood of the muscles fibres (only the left half of face is shown).

Figure 6: A schematic representation of stress stiffening effect. A point P inside a muscle at equilibrium under constant muscle activation (force F_1) (top panel) is virtually displaced by δ under the action of a transversal force F (bottom panel). Once the new equilibrium is reached with a new force level F_1, transversal stiffness $dF/d\delta$ is proportional to that force.

Figure 7: Modelling of the stress stiffening effect: variation of the hyperelastic constitutive law of the tissue with the activation of the muscle.

Figure 8: Face shaping after activation of the zygomaticus muscle

Figure 9: Face shaping from coordinate activation of the zygomaticus, levetor labii superioris alaeque nasi and levetor angulai oris muscles

Figure 10: Face shaping resulting from the orbicularis oris peripheralis activation

Figure 11: Face shaping resulting from the risorius activation

Figure 12: Face shaping resulting from the buccinator activation

Figure 13: Face shaping resulting from the orbicularis oris peripheralisand buccinator co-activation

Figure 14: Comparison between the trajectories of a point on the lower lip in the mid-sagittal plane in static and dynamic analysis resulting from an orbicularis oris peripheralis and mentalis co-activation (with E_{cable}=0.3 and T=-500 with spherical neighbourhood radius for OOP 3mm and for MENT 2 mm).

Figure 15: Upper panel: Velocity profile of a point on the lower lip in the mid-sagittal plane resulting from the co-activation of orbicularis oris peripheralis and mentalis in dynamic analysis. Lower panel: Time patterns of the corresponding activations. (with E_{cable}=0.3 and T=-500 with spherical neighbourhood radius for OOP 3mm and for MENT 2 mm)

Figure 16: Experimental data. Top panel: trajectory of a point on the lower lip in the mid-sagittal plane in /iRy/ sequence; diamond mark is for the starting point and square mark for the ending point. Bottom panel: corresponding acoustic signal with phonetic labelling

Figure 17: Experimental data. Tangential velocity profile corresponding to trajectory and the acoustic signal displayed in Figure 16.

TABLES

Table 1. Constants of the simplified 5-parameter Mooney-Rivlin model for passive tissues

c_{10} (MPa)	c_{20} (MPa)	d (1/MPa)
2.5e-3	1.175e-3	0.8

Table 2. Orofacial Muscles for half of the face

Muscle Name	Abbreviation	Number of Fibres	Total Number of Cable Elements
Levator Labii Superioris Alaeque Nasi	LLSAN	2	12
Levator Anguli Oris	LAO	1	9
Zygomaticus (major and minor)	ZYG	2	15
Risorius	RIS	1	6
Buccinator	BUC	2	12
Depressor Anguli Oris	DAO	2	12
Depressor Labii Inferioris	DLI	2	11
Mentalis	MENT	2	11
Orbicularis Oris Peripheralis (Inferioris and Superioris)	OOP	2	14
Orbicularis Oris Marginalis (Inferioris and Superioris)	OOM	2	14

Table 3. Tolerance values

	ε	V_{ref}
Force (N)	0.035	0.01
Displacement (mm)	0.01	0.00

REFERENCES

Abry C, Lallouache MT and Cathiard MA. 1996. How can coarticulation models account for speech sensitivity to audio-visual desynchronization? In Speechreading by Humans and Machines, NATO ASI Series F: Computer and System Sciences, Stork D & Hennecke M eds. 150:pp. 247-255. Springer-Verlag, Berlin, Heidelberg, Tokyo.

Ambadar Z, Schooler J and Cohn JF. 2005. Deciphering the enigmatic face: the importance of facial dynamics to interpreting subtle facial expressions. Psychological Science. 16(5): 403-41.

Ansys, Inc. 2007. Theory Reference Manual. Release 11.

Blanton PL, Biggs NL and Perkins RC. 1970. Electromyographic analysis of the buccinator muscle. J. Dent. Res. 49:389-394.

Badin P, Elisei F, Bailly G and Tarabalka Y. 2008. An audiovisual talking head for augmented speech generation: models and animations based on a real speaker's articulatory data. Proceedings of the 5th Conference on Articulated Motion and Deformable Objects (AMDO 2008). Springer Verlag LNCS 5098:132-143.

Blemker S, Pinsky PM and Delp SL. 2005. A 3D model of muscle reveals the causes of nonuniform strains in the biceps brachii. J. of Biomechanics. 38:657–665.

Buchaillard S, Perrier P and Payan Y. 2006. A 3D biomechanical vocal tract model to study speech production control: How to take into account the gravity? Proc. of the 7th International Seminar on Speech Production, pp. 403-410.

Buchaillard S, Perrier P and Payan Y. 2009. A biomechanical model of cardinal vowel production: Muscle activations and the impact of gravity on tongue positioning. J. Acoustical Society of America, 126(4):2033–2051.

Chabanas M, Luboz V and Payan Y. 2003. Patient specific finite element model of the face soft tissues for computer-assisted maxillofacial surgery. Medical Image Analysis. 7:131-151.

Feldman AG. 1986. Once more on the Equilibrium-Point hypothesis (λ model) for motor control. J. of Motor Behavior. 18(1):17-54.

Fung YC. 1993. Biomechanics: Mechanical properties of living tissues. Springer-Verlag, New York Inc.

Gerard JM, Ohayon J, Luboz V, Perrier P and Payan Y. 2005. Non-linear elastic properties of the lingual and facial tissues assessed by indentation technique, Application to the biomechanics of speech production. Medical Engineering & Physics. 27:884-892.

Gladilin E, Ivanov A and Roginsky V. 2004. A framework for biomechanical simulation of cranio-maxillofacial surgery interventions. Proc of International Symposium on Medical Simulation, ISMS 2004, S. Cotin and D. Metaxas, eds., pp. 287-294.

Gomi H, Nozoe J, Dang J and Honda K. 2006. A physiologically based model of perioral dynamics for various lip deformations in speech articulation. Speech Production: Models, Phonetic Processes and Techniques, J. Harrington and M. Tabain, eds., Psychology Press, pp 119-134.

Groleau J, Chabanas M, Marécaux Ch, Payrard N, Segaud B, Rochette M, Perrier P and Payan Y. 2007. A biomechanical model of the face including muscles for the prediction of deformations during speech production. Proceedings of the 5th International Workshop on Models and Analysis of Vocal Emissions for Biomedical Applications, MAVEBA'2007, Firenze, Italie.

Hardcastle WJ. 1976. Physiology of Speech Production. Academic Press, London.

Hill AV. 1938. The heat of shortening and the dynamic constants of muscle. Proc Royal Society, Biological Sciences. 126:136-195.

Humphrey JD and Yin FCP. 1989. Constitutive relations and finite deformations of passive cardiac tissue II: Stress analysis in the left ventricle. Circulation Research. 65:805-817.

Lee Y, Terzopoulos D and Waters K. 1995. Realistic modeling for facial animation. SIGGRAPH'95, S.G. Mair and R. Cook, eds. New York, ACM Press, 55–62.

Loocke MV, Lyons CG and Symms CK. 2006. A validated model of passive muscle in compression. J. of Biomechanics. 39:2999-3009.

Lucero JC and Munhall KG. 1999. A model of facial biomechanics for speech production. J. Acoust. Soc. Am. 106:2834–2842.

Lucero JC, Maciel STR, Johns DA and Munhall KG. 2005. Empirical modeling of human face kinematics during speech using motion clustering. J. Acoust. Soc. Am. 118(1): 405-409.

McGurk H and MacDonald J. 1976. Hearing Lips and Seeing Voices. Nature, 264746-48.

McMahon TA. 1984. Muscles, Reflexes, and Locomotion. Princeton University Press.

Morasso P. 1981. Spatial control of arm movements. Exp. Brain Res. 42:223-227.

Munhall KG and Vatikiotis-Bateson E. 1998. The moving face during speech communication. Hearing by Eye, Part 2: The Psychology of Speechreading and Audiovisual Speech, edited by R. Campbell, B. Dodd, and D. Burnham. Taylor and Francis, Psychology Press, London.

Nazari MA, Payan Y, Perrier P, Chabanas M and Lobos C. 2008. A continuous biomechanical model of the face: a study of muscle coordinations for speech lip gestures. Proceedings of the 8th International Seminar on Speech Production, ISSP'08, pp. 321-324.

Ng-Thow-Hing V and Fiume E. 2002. Application-specific muscle representations. Proc. of Gr. Inter, W. Sturzlinger and M. McCool, editors, pp. 107–115.

O'Shaughnessy D. 1081. A study of French vowel and consonant durations. J. of Phonetics. 9:385-406.

Payan Y and Perrier P. 1997. Synthesis of V-V sequences with a 2D biomechanical tongue model controlled by the Equilibrium Point Hypothesis. Speech Communication. 22:185-205.

Perrier P, Payan Y, Zandipour M and Perkell J. 2003. Influences of tongue biomechanics on speech movements during the production of velar stop consonants: A modeling study. J. Acoustical Soc. of America. 114(3):77–83.

Shaiman S, Adams SG and Kimelman MDZ. 1997. Velocity profiles of lip protrusion across changes in speaking rate. Journal of Speech, Language, and Hearing Research. 40: 144-158.

Sifakis E, Neverov I and Fedkiw R. 2005. Automatic Determination of Facial Muscle Activations from Sparse Motion Capture Marker Data. ACM Transactions on Graphics (SIGGRAPH Proceedings).24:417-425.

Sifakis E, Selle A, Robinson-Mosher A and Fedkiw R. 2006. Simulating Speech with a Physics-Based Facial Muscle Model. Eurographics/ ACM SIGGRAPH, M.P. Cani, and J.O. Brien, editors, Symposium on Computer Animation.

Standring S. (editor in chief). 2005. Gray's Anatomy: The Anatomical Basis of Clinical Practice. 39th Edition, Elsevier Ltd..

Teran J, Sifakis E, Blemker S, Ng Thow Hing V, Lau C and Fedkiw R. 2005. Creating and Simulating Skeletal Muscle from the Visible Human Data Set. IEEE TVCG. 11:317-328.

Tracqui P and Ohayon J. 2004. Transmission of mechanical stresses within the cytoskeleton of adherent cells: a theoretical analysis based on a multi-component model. Acta Biotheoretica. 52:323-341.

Weiss JA, Maker BN and Govindjee S. 1996. Finite element implementation of incompressible, transversely isotropic hyperelasticity. Comput. Methods Appl. Mech. Engrg. 135:107-128.

Wilhelms-Tricario R. 1995. Physiological modeling of speech production: methods for modeling soft-tissue articulators. J. Acoustical Society of America. 97:3085–3098.

Yucesoy CA, Koopman BHFJM, Huijing PA and Grootenboer HJ. 2002. Three-dimensional finite element modeling of skeletal muscle using a two-domain approach: linked fibre-matrix mesh model. J. of Biomechanics. 35:1253-1262.

Zajac F. 1989. Muscle and tendon: Properties, models, scaling, and application to biomechanics and motor control. Critical Reviews in Biomed. Eng. 17:359–411.

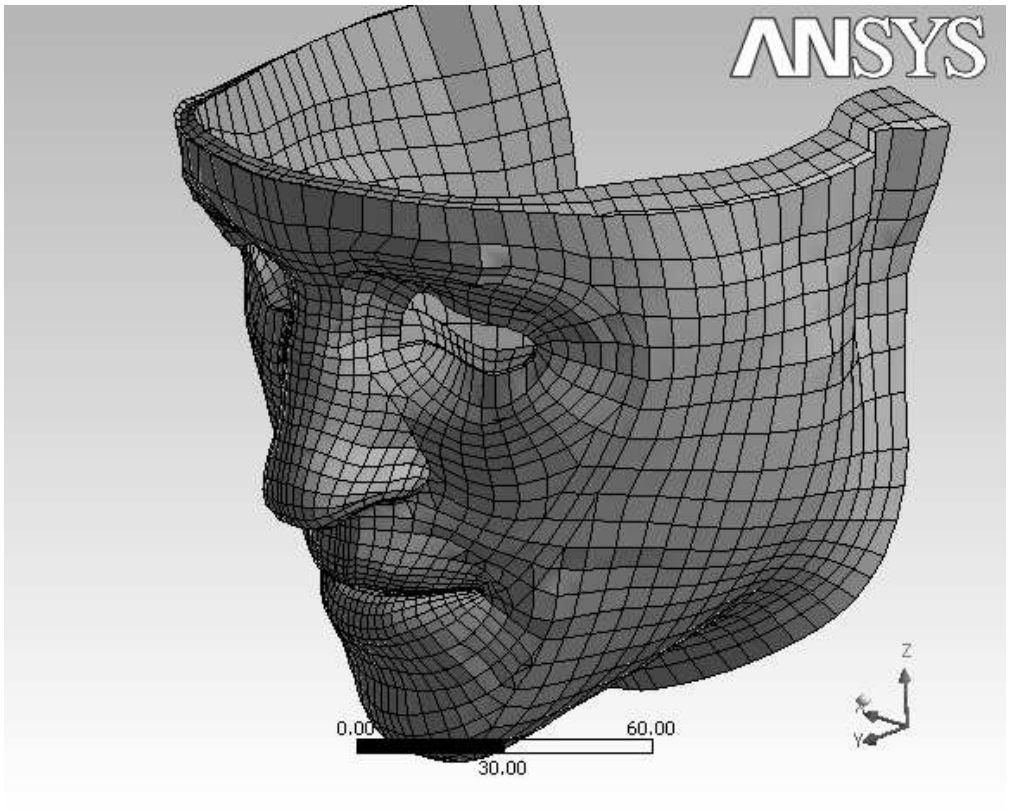

Figure 1: Main mesh of the face soft tissue.
204x164mm (72 x 72 DPI)

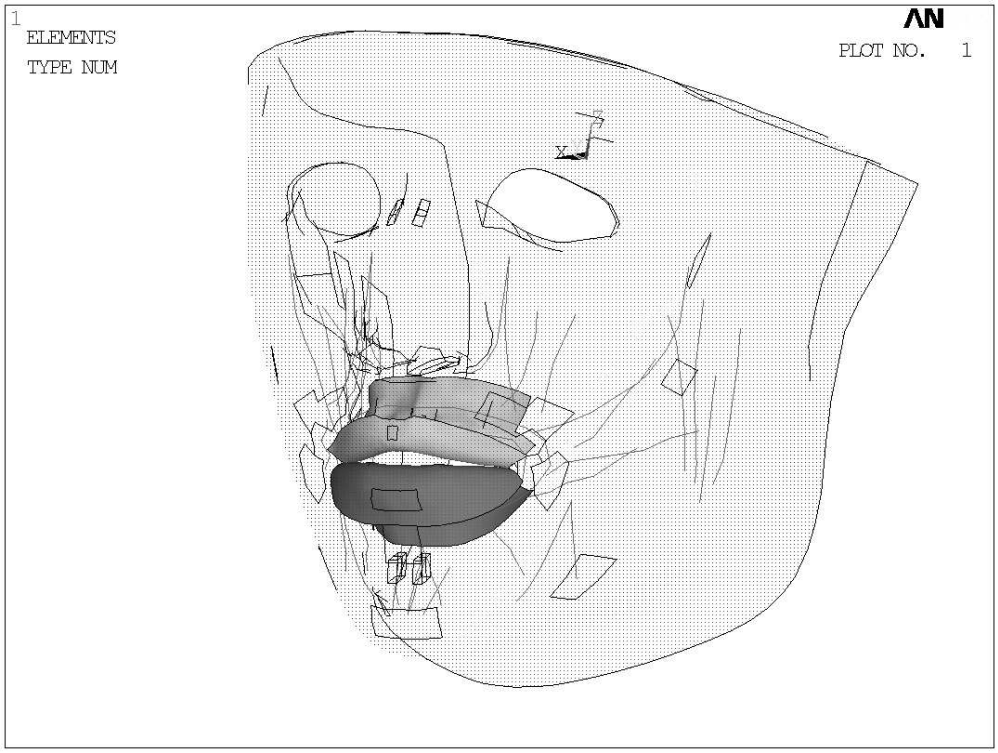

Figure 2: Surfaces of contact elements between lips (a)
379x285mm (72 x 72 DPI)

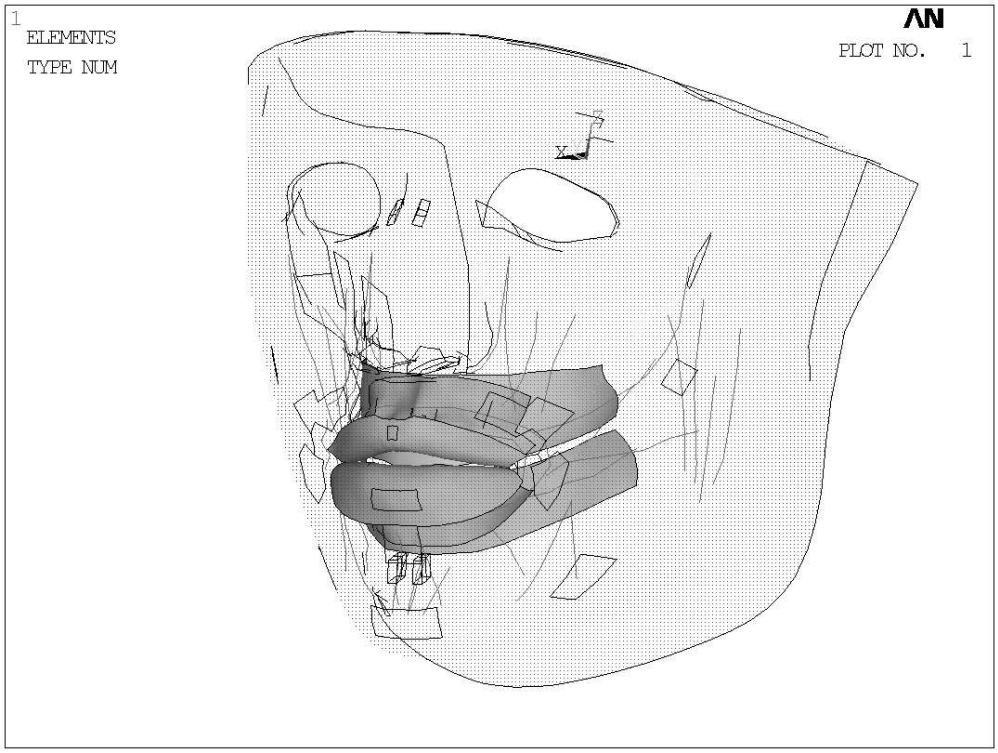

and lips and teeth (b).
379x285mm (72 x 72 DPI)

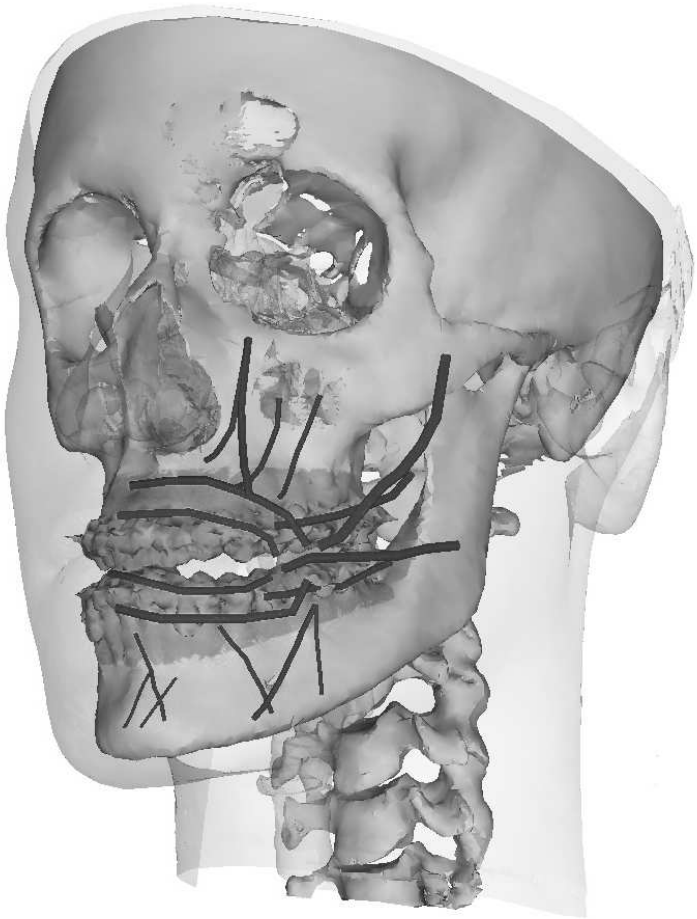

Figure 3: Macrofibers defining the muscles of the face shown in CT data (a), 340x351mm (72 x 72 DPI)

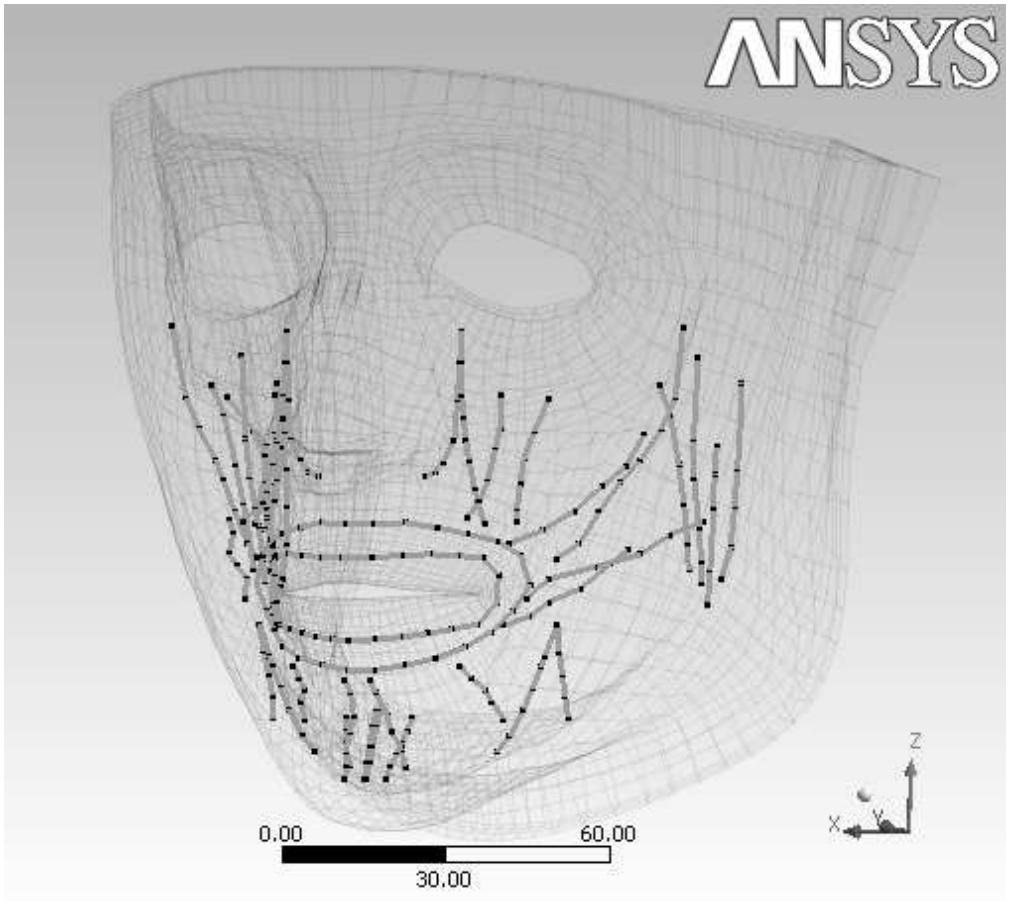

in the main mesh (b),
178x160mm (72 x 72 DPI)

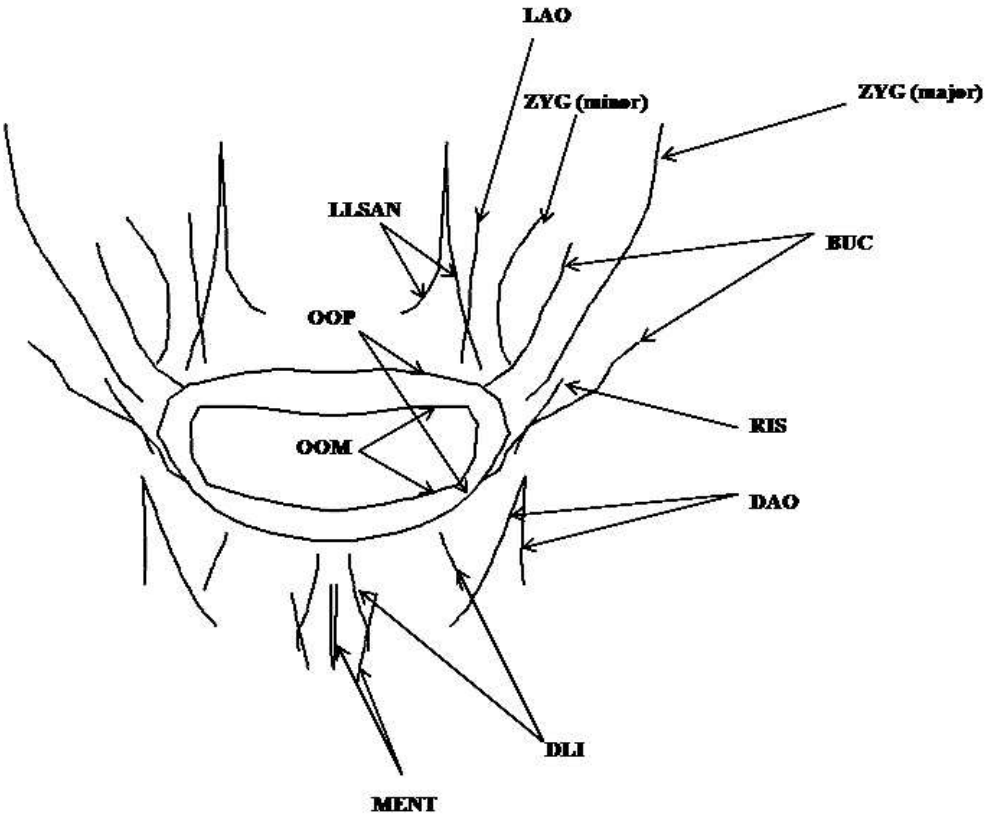

and with their abbreviated names (c).
245x202mm (72 x 72 DPI)

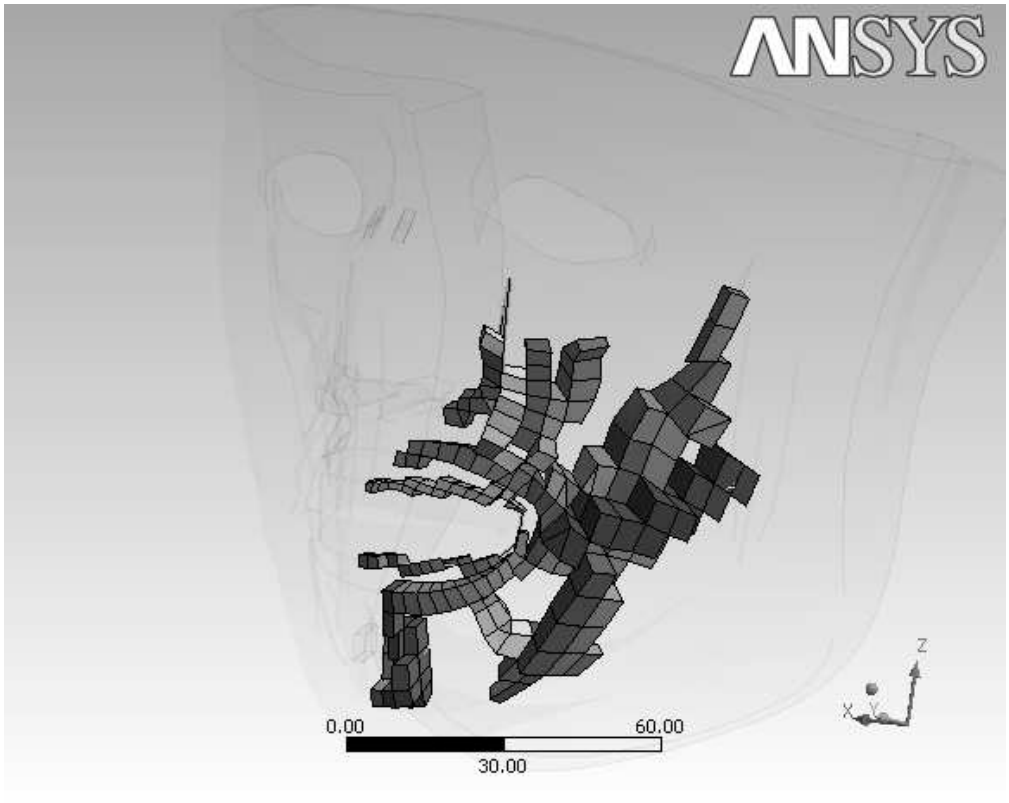

Figure 4: Coupling elements between the piece-wise fibres of cable elements and the main mesh (only the left half of face is shown).
204x164mm (72 x 72 DPI)

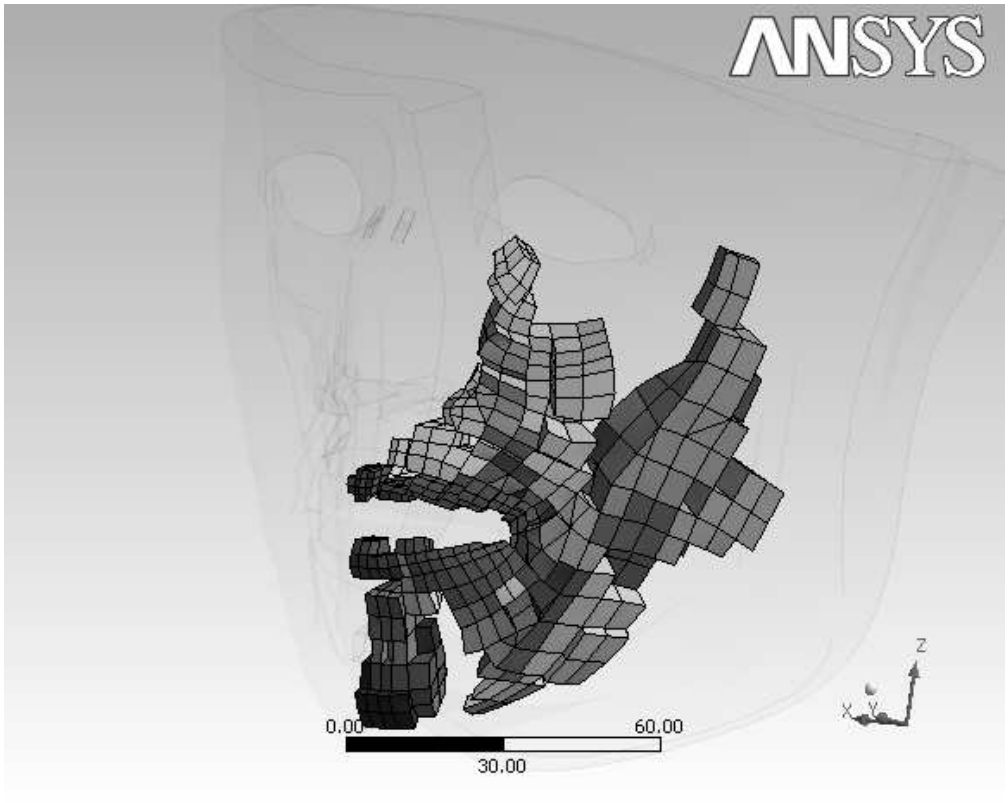

Figure 5: Body of the muscles: elements of the main mesh in a neighbourhood of the muscles fibres (only the left half of face is shown).
204x164mm (72 x 72 DPI)

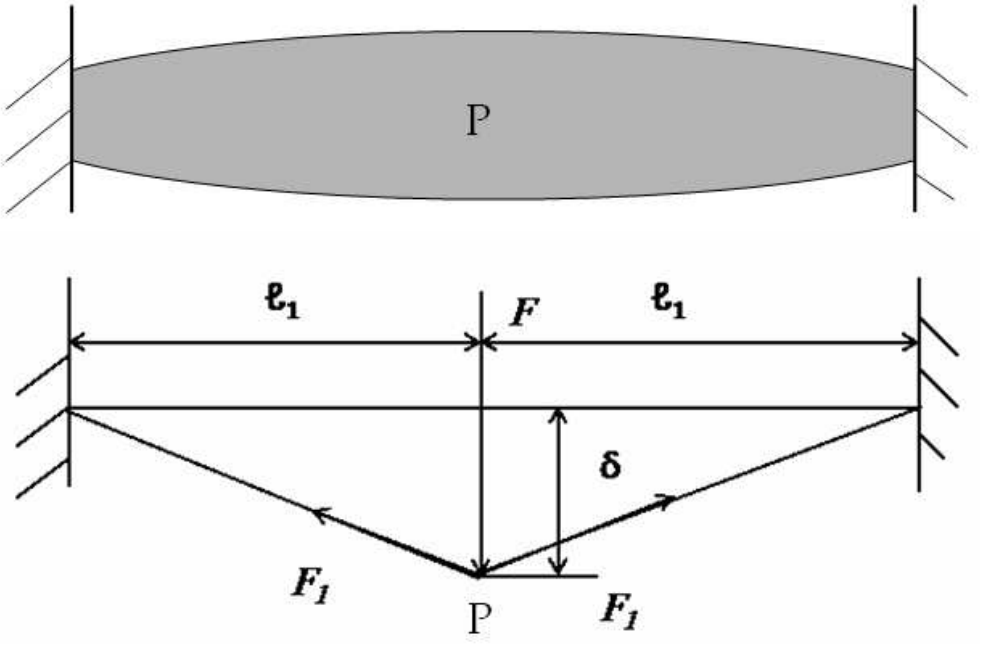

Figure 6: A schematic representation of stress stiffening effect. A point P inside a muscle at equilibrium under constant muscle activation (force F1) (top panel) is virtually displaced by δ under the action of a transversal force F (bottom panel). Once the new equilibrium is reached with a new force level F1, transversal stiffness dF/dδ is proportional to that force.
219x144mm (72 x 72 DPI)

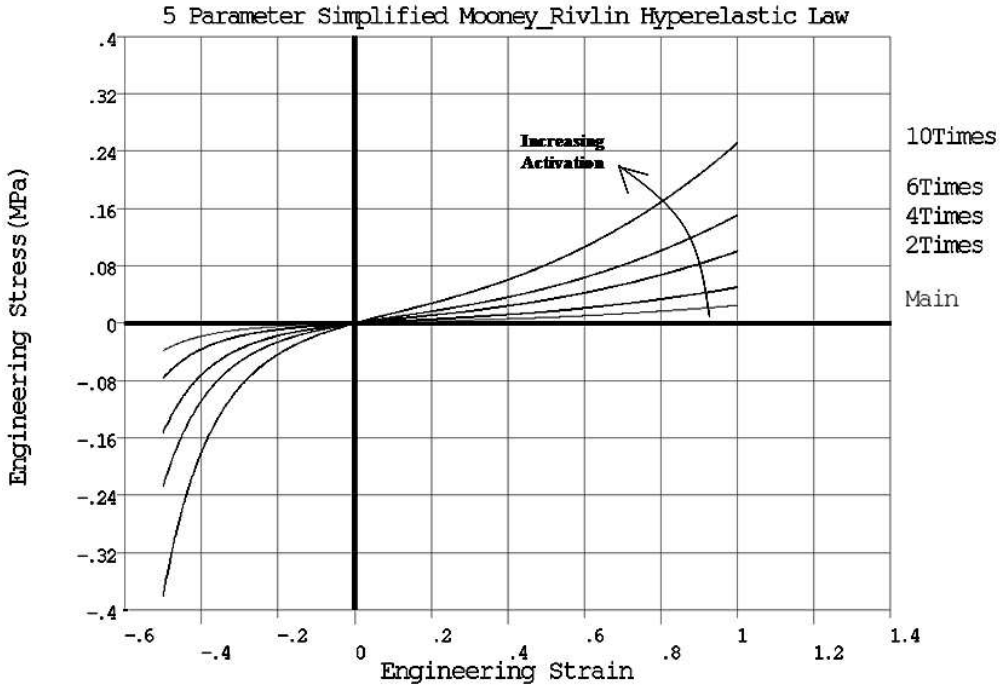

Figure 7: Modelling of the stress stiffening effect: variation of the hyperelastic constitutive law of the tissue with the activation of the muscle.
291x206mm (72 x 72 DPI)

Figure 8: Face shaping after activation of the zygomaticus muscle
759x285mm (72 x 72 DPI)

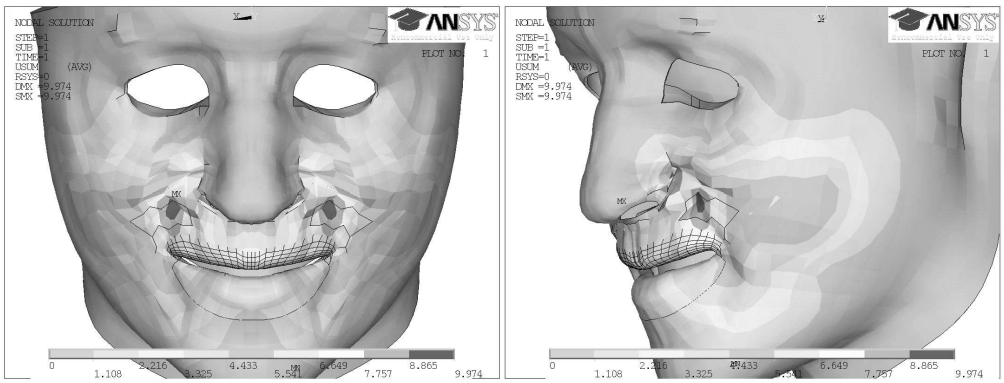

Figure 9: Face shaping from coordinate activation of the zygomaticus, levetor labii superioris alaeque nasi and levetor angulai oris muscles
759x285mm (72 x 72 DPI)

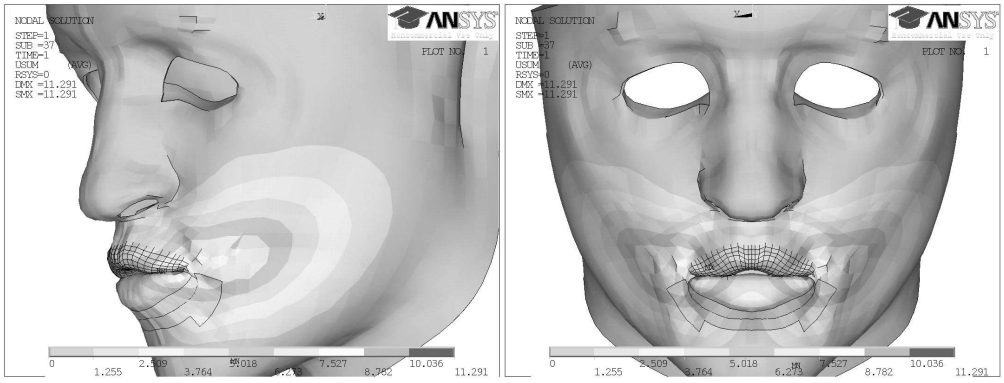

Figure 10: Face shaping resulting from the orbicularis oris peripheralis activation
759x285mm (72 x 72 DPI)

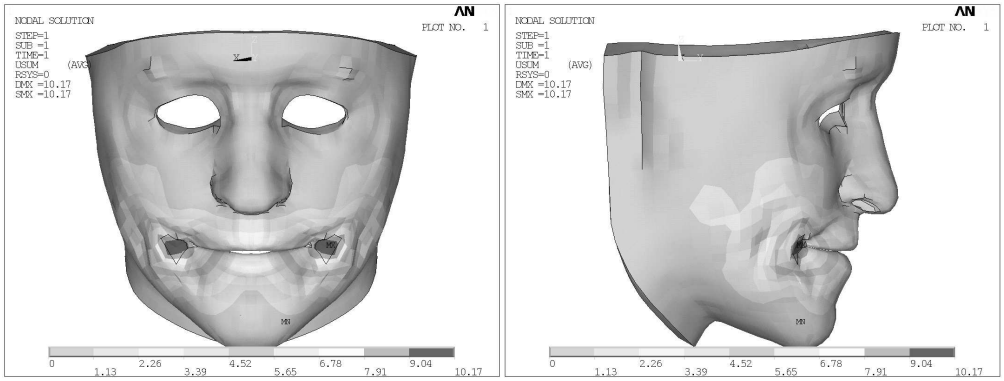

Figure 11: Face shaping resulting from the risorius activation
759x285mm (72 x 72 DPI)

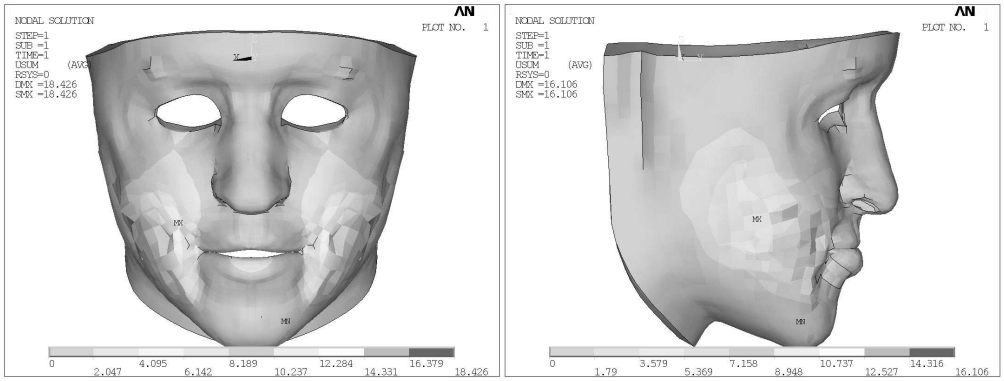

Figure 12: Face shaping resulting from the buccinator activation
759x285mm (72 x 72 DPI)

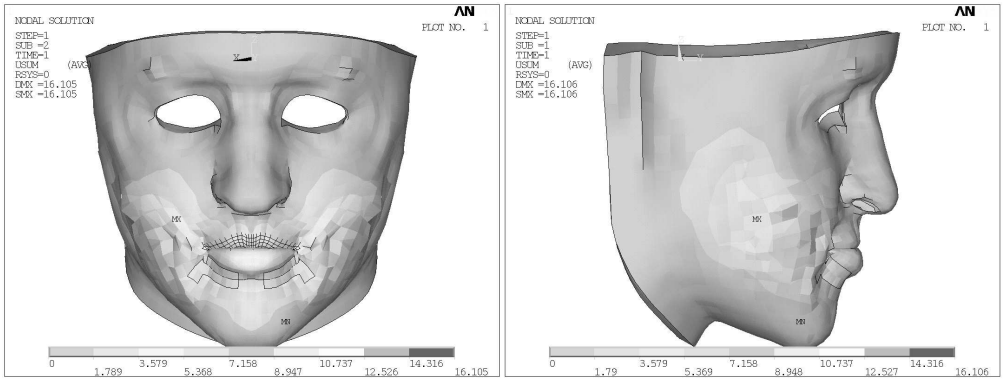

Figure 13: Face shaping resulting from the orbicularis oris peripheralisand buccinator co-activation
759x285mm (72 x 72 DPI)

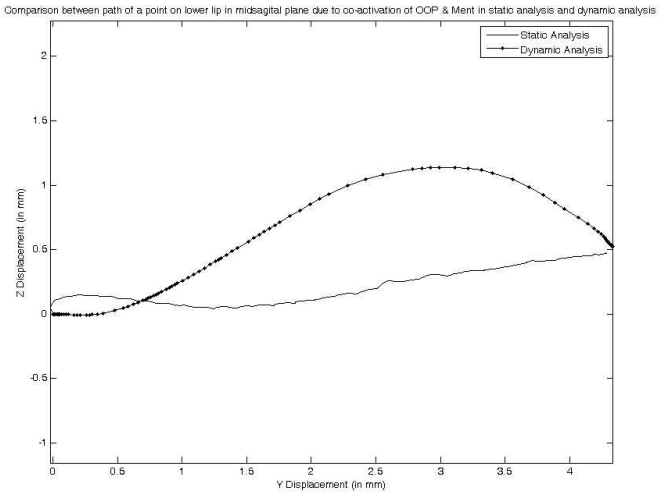

Figure 14: Comparison between the trajectories of a point on the lower lip in the mid-sagittal plane in static and dynamic analysis resulting from an orbicularis oris peripheralis and mentalis co-activation (with Ecable=0.3 and T=-500 with spherical neighbourhood radius for OOP 3mm and for MENT 2 mm).
338x184mm (96 x 96 DPI)

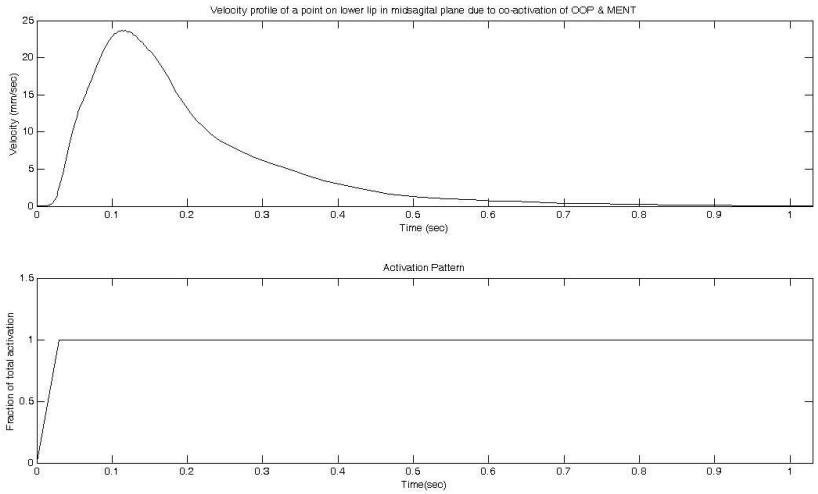

Figure 15: Upper panel: Velocity profile of a point on the lower lip in the mid-sagittal plane resulting from the co-activation of orbicularis oris peripheralis and mentalis in dynamic analysis. Lower panel: Time patterns of the corresponding activations. (with Ecable=0.3 and T=-500 with spherical neighbourhood radius for OOP 3mm and for MENT 2 mm).
338x184mm (96 x 96 DPI)

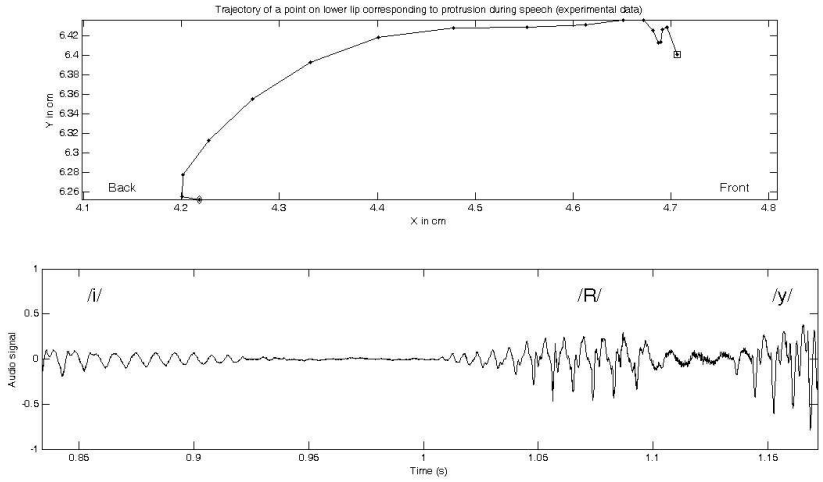

Figure 16: Experimental data. Top panel: trajectory of a point on the lower lip in the mid-sagittal plane in /iRy/ sequence; diamond mark is for the starting point and square mark for the ending point. Bottom panel: corresponding acoustic signal with phonetic labelling.
338x178mm (96 x 96 DPI)

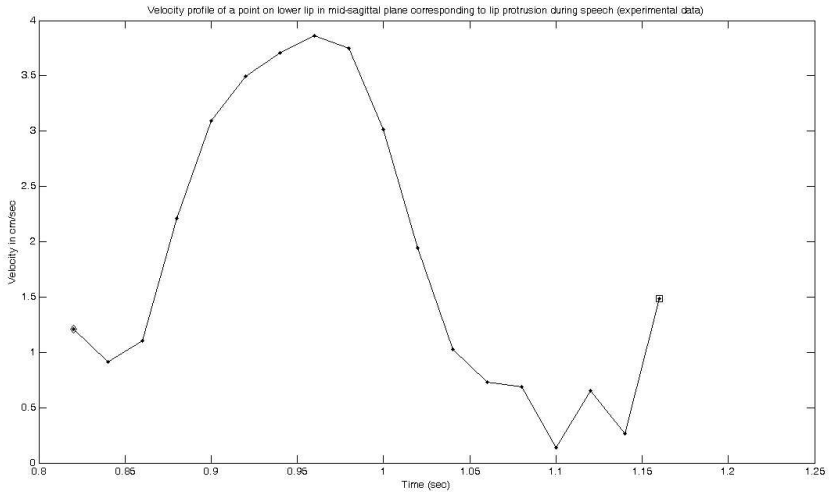

Figure 17: Experimental data. Tangential velocity profile corresponding to trajectory and the acoustic signal displayed in Figure 16.
338x184mm (96 x 96 DPI)